JOURNAL OF TISSUE ENGINEERING AND REGENERATIVE MEDICINE
J Tissue Eng Regen Med 2016.
Published online in Wiley Online Library (wileyonlinelibrary.com) **DOI:** 10.1002/term.2227

RESEARCH ARTICLE

Silk fibroin scaffolds with muscle-like elasticity support *in vitro* differentiation of human skeletal muscle cells

Vishal Chaturvedi[1], Deboki Naskar[2], Beverley F. Kinnear[1], Elizabeth Grenik[4], Danielle E. Dye[1], Miranda D. Grounds[3], Subhas C. Kundu[2*,†] and Deirdre R. Coombe[1*]

[1]*School of Biomedical Science, CHIRI Biosciences Research Precinct, Faculty of Health Sciences, Curtin University, Perth, Western Australia*
[2]*Department of Biotechnology, Indian Institute of Technology, Kharagpur, West Bengal, India*
[3]*School of Anatomy, Physiology and Human Biology, University of Western Australia, Perth, Western Australia*
[4]*Nanochemistry Research Institute, Faculty of Science, Engineering and Computing, Curtin University, Perth, Western Australia*

Abstract

Human adult skeletal muscle has a limited ability to regenerate after injury and therapeutic options for volumetric muscle loss are few. Technologies to enhance regeneration of tissues generally rely upon bioscaffolds to mimic aspects of the tissue extracellular matrix (ECM). In the present study, silk fibroins from four Lepidoptera (silkworm) species engineered into three-dimensional scaffolds were examined for their ability to support the differentiation of primary human skeletal muscle myoblasts. Human skeletal muscle myoblasts (HSMMs) adhered, spread and deposited extensive ECM on all the scaffolds, but immunofluorescence and quantitative polymerase chain reaction analysis of gene expression revealed that myotube formation occurred differently on the various scaffolds. *Bombyx mori* fibroin scaffolds supported formation of long, well-aligned myotubes, whereas on *Antheraea mylitta* fibroin scaffolds the myotubes were thicker and shorter. Myotubes were oriented in two perpendicular layers on *Antheraea assamensis* scaffolds, and scaffolds of *Philosamia/Samia ricini (S. ricini)* fibroin poorly supported myotube formation. These differences were not caused by fibroin composition *per se*, as HSMMs adhered to, proliferated on and formed striated myotubes on all four fibroins presented as two-dimensional fibroin films. The Young's modulus of *A. mylitta* and *B. mori* scaffolds mimicked that of normal skeletal muscle, but *A. assamensis* and *S. ricini* scaffolds were more flexible. The present study demonstrates that although myoblasts deposit matrix onto fibroin scaffolds and create a permissive environment for cell proliferation, a scaffold elasticity resembling that of normal muscle is required for optimal myotube length, alignment, and maturation.

Received 7 October 2015; Revised 23 March 2016; Accepted 21 April 2016

Keywords **silk fibroin; extracellular matrix; primary human myoblasts; myotubes; skeletal muscle tissue engineering; biomaterials; elasticity**

1. Introduction

When skeletal muscle is damaged and undergoes myofibre necrosis, the satellite (progenitor) cells of skeletal muscle are activated to proliferate, differentiate and fuse to form mature myotubes. However, when large amounts of muscle become necrotic or are lost, such as in battlefield injuries or car accidents, this classic regenerative response is not sufficient to repair the defect (Grogan *et al*., 2011). Current therapies such as muscle grafts to replace lost muscle mass are not ideal because of donor site morbidities, and strategies to enhance endogenous repair of muscle also have limitations (reviewed in Grounds, 2014). Recently, the efficacy of acellular bioscaffolds to stimulate new muscle formation *in vivo*, or the *ex vivo* formation of muscle-like structures for subsequent implantation have been explored (Wang *et al*., 2014). At present, one of the most successful bioscaffolds reported in clinical skeletal muscle repair is decellularized porcine extracellular matrix (ECM) derived from small intestine or bladder. These scaffolds have been implanted in load-bearing limb muscles and, in combination with physical therapy, have resulted in functional improvement in human patients, albeit in small studies (Mase *et al*., 2010; Gentile *et al*., 2014; Sicari *et al*., 2014). Although numerous studies have examined different bioscaffolds for their compatibility with muscle cells *in vitro*, these have generally used the murine myoblast cell line C2C12. The use of primary human skeletal muscle myoblasts (HSMMs) to test the cytocompatibility of different scaffolds is an essential first step to assess their viability for human muscle bioengineering.

Silk is a biopolymer produced by the silk glands of arthropods with the main source being the larvae of various Lepidoptera silkworms. Two major groups of silkworm are of commercial importance: Bombycidae (mulberry) and Saturniidae (non-mulberry) (Mahendran *et al*., 2006). The domesticated mulberry species *Bombyx mori* is widely distributed, whereas the commercially available non-

*Correspondence to: D.R. Coombe, E-mail: d.coombe@curtin.edu.au and S.C. Kundu, E-mail: kundu@hijli.iitjgp.erne
†Present address: 3Bs Research Group, Headquarters of the European Institute of Excellence on Tissue Engineering and Regenerative Medicine, University of Minho, AvePark - 4805-017 Barco, Guimaraes, Portugal

mulberry varieties *Antheraea mylitta* (Tropical Tasar), *Antheraea assamensis/assama* (Muga) and *Philosamia/ Samia ricini* (Eri) are all from the Indian subcontinent.

There are two types of silk proteins obtained from the cocoons of *B. mori*: a water-soluble protein called sericin and a fibrous hydrophobic protein called fibroin. Fibroin is the key component of silk from *B. mori* and consists of a heavy (H) chain (390 kDa) and a light (L) chain (26 kDa) connected by a disulphide bond (Zhou *et al*., 2000). A 30 kDa glycoprotein (P25) is non-covalently linked to the H–L chain complex through hydrophobic interactions (Tanaka *et al*., 1999). The H chain comprises a highly repetitive glycine-rich core, flanked by non-repetitive sequences. These glycine motifs form highly ordered β-sheets which gives rise to the strength and toughness of silk, while the non-crystalline regions contribute flexibility and elasticity (Fu *et al*., 2009).

Fibroin proteins from non-mulberry silkworm species have slightly different structures. *Antheraea mylitta* is a homodimer containing 197 kDa subunits, *A. assamensis* fibroin is a heterodimer comprising chains of 220 kDa and 20 kDa, and fibroin from *S. ricini* consists of a heterodimer of chains of approximately 245 kDa and 210 kDa (Kundu *et al*., 2012b; Pal *et al*., 2013). Non-mulberry silk also contains poly-alanine rather than poly-glycine repeats and is more hydrophobic than *B. mori* silk (Kundu *et al*., 2012a). In addition, fibroin from *A. mylitta* contains the integrin binding motif arginine–glycine–aspartic acid (RGD), whereas the others do not (Morgan *et al*., 2008).

Properties such as high tensile strength, elasticity, thermal stability, aqueous preparation, slow degradability and biocompatibility make silk a useful biomaterial. Silk proteins are used in implantable biomaterials, drug delivery vehicles and medical devices (Omenetto and Kaplan, 2010; Kundu *et al*., 2013, Yucel *et al*., 2014). Although silk from *B. mori* is the most commonly used in medical applications, attention is gradually focusing on silk produced by non-mulberry species, as these fibroins can be easily extracted in aqueous solution (Patra *et al*., 2012; Kar *et al*., 2013; Pal *et al*., 2013). Silk biomaterials can be moulded into hydrogels, membranes, nets, sponges, micro and nanoparticles and nanofibrous mats, (Kundu *et al*., 2012b) and can be used for different tissue engineering applications including bone (Meinel *et al*., 2005; Kim *et al*., 2008; Meinel and Kaplan, 2012), cartilage (Bhardwaj *et al*., 2011; Talukdar *et al*., 2011), cardiac muscle (Patra *et al*., 2012), liver (Banani and Kundu, 2013) and skin repair (Bhardwaj *et al*., 2015). Silk scaffolds biodegrade without the release of toxic products both *in vitro* (Horan *et al*., 2005; Li *et al*., 2003) and *in vivo* (Wang *et al*., 2008; Zhou *et al*., 2010), and are associated with transient but not chronic inflammation when implanted into rats (Wang *et al*., 2008). *In vitro* studies have also shown that silk fibroin films can support growth of a large number of cell types, including C2C12 mouse myoblasts (Park *et al*., 2013a) and MG-63 osteoblast like cells (Kar *et al*., 2013), whereas three-dimensional (3D) porous silk fibroin scaffolds have been used to culture rat neonatal cardiomyocytes (Patra *et al*., 2012) and cortical neuronal cells (Tang-Schomer *et al*., 2014).

Although a wide range of materials have been investigated as bioscaffolds for skeletal muscle formation and repair, few studies have used silk (see Table 1), and none have tested the response of primary human skeletal muscle cells. This aim of this study was to explore the capacity of 3D scaffolds engineered from different mulberry and non-mulberry silk fibroins derived from four Lepidoptera species (*B. mori, A. mylitta*, *A. assamensis* and *P./S. ricini)* to support myoblast proliferation, differentiation and myotube formation. It was hypothesized that human myoblasts would behave differently on the different silk scaffolds. The response of human myoblasts to solubilized silk fibroins in two-dimensions (2D) was also examined, to investigate if differences in myoblast maturation resulted from the chemical composition of the fibroins or the 3D structural properties of the scaffolds. Striking differences were observed in the way the human muscle cells responded to the different silk fibroin substrates.

2. Materials and methods

All reagents and chemicals were purchased from Sigma-Aldrich (St Louis, MO, USA), unless otherwise stated.

Table 1. Previous *in vitro* studies of myoblast growth and differentiation using silk protein matrices

Silk matrix type	Cell type	Experiment	Outcome	Reference
Fibroin*–polyurethane blended films	C2C12 mouse myoblasts	Compatibility and differentiation	Silk fibroin improved the cell compatibility of polyurethane films	Park et al. (2013b)
Fibroin* immobilized on polyurethane membranes	Cells from skeletal muscle biopsy (primary hypopharynx myoblasts)	Compatibility and differentiation	Cell proliferation, alignment and myofibre differentiation achieved in aligned microchannels	Shen *et al*. (2013)
Fibroin*–tropoelastin films	C2C12 cells and human bone marrow stem cells (hMSCs)	Cell attachment, proliferation and myogenic lineage differentiation	Roughness & stiffness favouring proliferation and differentiation of C2C12 cells or hMSCs determined	Hu *et al*. (2011)
Recombinant spider silk protein eADF4(C16) film	C2C12 mouse myoblasts	Cell adhesion and orientation	Myoblasts adhered to and proliferated best on structured, not unstructured films	Bauer *et al*. (2013)
Sericin* supplemented serum-free medium	C2C12 mouse myoblasts	Myoblast differentiation	Myotubes formed with sarcomeres	Fujita *et al.*, 2010 (Fujita *et al*., 2010)

*Silk protein obtained from *Bombyx mori*, a mulberry silkworm species.

DOI: 10.1002/term

2.1. Collection of mulberry and non-mulberry silkworm species

Bombyx mori cocoons were collected from Debra Sericulture Farm, West Midnapore, West Bengal, India. *Antheraea mylitta* fifth instar mature larvae were collected from the Indian Institute of Technology (IIT) Kharagpur Farm. Both *A .assamensis* and *S. ricini* fifth instar larvae were collected from Coochbehar, West Bengal, India.

2.2. Processing of silk protein fibroin into 3D scaffolds

The methods used to prepare the regenerated fibroin solutions are outlined in Figure 1. Briefly, fibroin was isolated from *B. mori* cocoons using a protocol described elsewhere (Sofia *et al*., 2001). Fibroins from the non-mulberry species were isolated by squeezing the glands of fifth instar larvae immediately prior to them spinning their cocoons following the steps described elsewhere (Datta *et al*., 2001a; Kar *et al*., 2013; Pal *et al*., 2013). Fibroin solutions (2% *w/v*ol) were used to fabricate 3D porous sponges/scaffolds using the freeze drying technique described in Nazarov *et al*. (2004). The scaffolds (14 mm in diameter and 4 mm high) were fixed with 90% ethanol for 1 h and then, for 30 min each, with 70% and 50% ethanol. Scaffolds were washed twice in phosphate-buffered saline (PBS) for 30 min, placed under ultraviolet (UV) light for 20 min and then into the wells of a 24-well plate and preconditioned in Skeletal Muscle Growth Medium-2 (SkGM-2; Lonza, Basel, Switzerland) for 2 h at 37°C.

2.3. Solubilization of the silk fibroin from freeze dried scaffolds for 2D culture

All silk fibroin scaffolds were solubilized in PBS. Scaffolds were placed in 1.5 ml tubes, 500 µl of PBS was added and incubation proceeded at 42°C for 30 min with rocking. Supernatants collected after centrifugation at

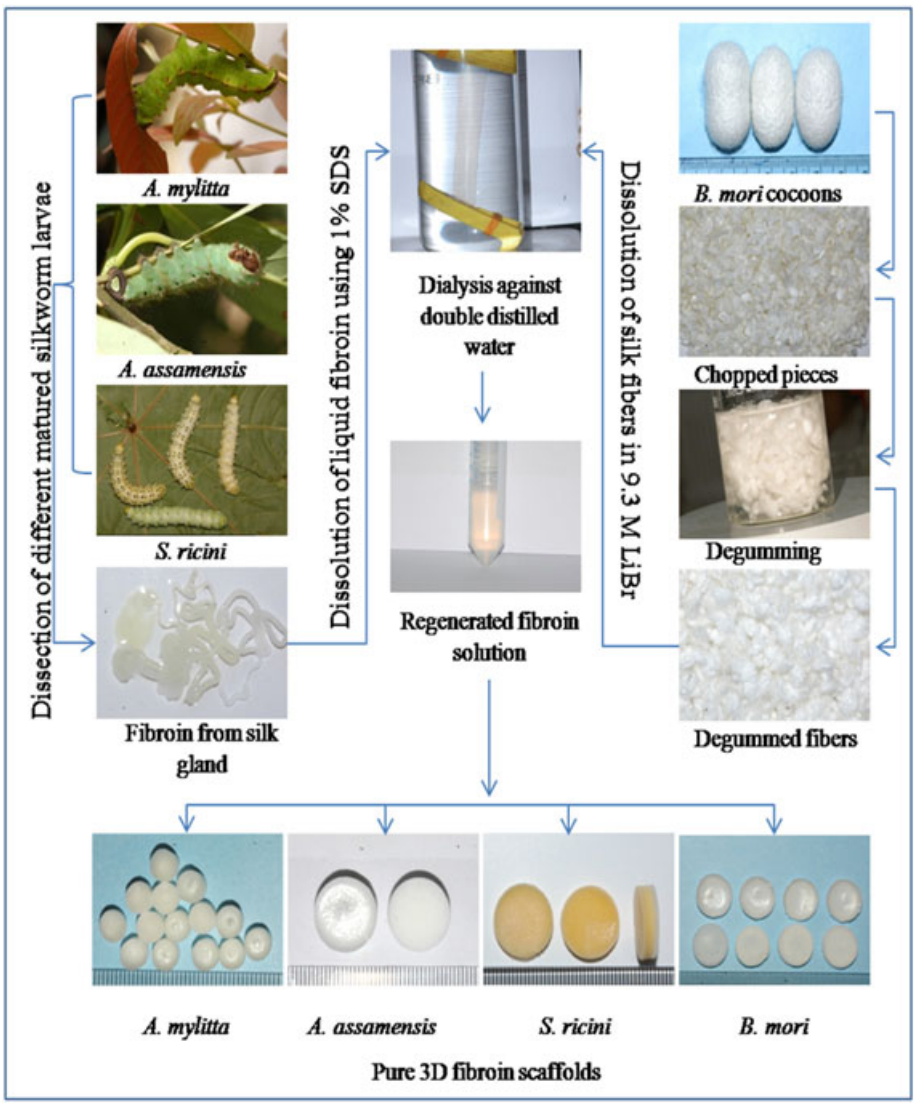

Figure 1. Schematic representation of silk protein fibroin isolation from mulberry and non-mulberry silkworm species and the preparation of three-dimensional (3D) fibroin scaffolds. SDS, sodium dodecyl sulphate

DOI: 10.1002/term

9000 rpm for 10 min at 4° C were centrifuged again and their protein content measured using a BCA protein assay kit (Pierce Biotechnology, Rockford, IL, USA). The solubilized silk was stored at 4° C. Routinely, 10 μg/cm^2 silk fibroin was used to coat tissue culture plastic or etched glass surfaces.

2.4. Antibodies

Rabbit polyclonal antibodies against fibronectin and glucose transporter 4 (GLUT4) were purchased from Abcam (Cambridge, UK). The anti-perlecan rabbit polyclonal antibody was a gift from Prof. John Whitelock (University of NSW, Sydney, Australia). Anti-myosin [slow skeletal heavy chain (MyHCB), clone NOQ7.5.4D] mouse monoclonal antibody (mAb) was purchased from Millipore (Temecula, CA, USA). Secondary antibodies were goat anti-rabbit Alexa Fluor 546 (AF546), goat anti-mouse Alexa Fluor 488 (AF488) and goat anti-rabbit AF488 (all Molecular Probes, Life Technologies, Eugene, OR, USA). Primary antibodies were used at concentrations of 2–4 μg per test. The control antibodies were rabbit IgG and mouse IgG (Zymed; Life Technologies).

2.5. Cell culture

The HSMMs (derived from a single donor) were purchased from Lonza (catalogue number CC-2580) and maintained in a humidified 37°C incubator equilibrated at 5% CO_2 in SkGM-2 (Lonza) containing human epidermal growth factor (EGF), dexamethasone, L-glutamine and 10% fetal bovine serum (FBS). The HSMMs were passaged at 50–70% confluence and cells from less than five passages were used in experiments.

2.6. Proliferation and differentiation of HSMMs on 3D scaffolds

The HSMMs in SkGM-2 medium (7.5×10^4 cells in 25 μl) were added to scaffolds and allowed to adhere at 37°C for 30 min, after which cells and scaffolds were transferred to new wells and 2 ml of SkGM-2 medium was added. Cells were grown for 5 days with medium replenished on day 3. The scaffolds were fixed and processed either for scanning electron microscopy (SEM) or stained with rhodamine–phalloidin, 10 Units/ml (Molecular Probes), in PBS for confocal microscopy. To assess differentiation, HSMMs in SkGM-2 medium (5×10^5 cells in 25 μl) were added to scaffolds as described above. After 4 days of culture, the medium was changed to Dulbecco's Modified Eagle Medium (DMEM)/F10/2% horse serum (HS) to trigger differentiation. Cells were cultured for a further 10 or 11 days with medium replacement every third day, then fixed, permeabilized and stained with anti-MyHCB mAb as described previously.

2.7. Immunofluorescence of matrix proteins

The HSMMs in SkGM-2 medium were seeded on 3D silk scaffolds (7.5×10^4 cells/cm^2) and cultured for 3 days. The scaffolds were washed and fixed with 4% paraformaldehyde (PFA)/PBS, then incubated in blocking solution for 1 h at room temperature (RT). Following washing with PBS they were incubated for 2 h at RT in a polyclonal antibody recognizing either fibronectin or perlecan, then washed with PBS and incubated in secondary antibody (anti-rabbit AF488). All antibodies were diluted in blocking solution. The scaffolds were washed and mounted in Vectashield (Vector Laboratories, Burlingame, CA, USA). The images were captured with a A1+ confocal microscope (Nikon, Tokyo, Japan) using NIS-Elements AR analysis version 4.10 software (Nikon, Tokyo, Japan). All images were acquired at the same gain and exposure settings.

2.8. Confocal laser scanning microscopy of scaffolds

To generate a single image, 15–25 z-stack images (2, 5 or 10 μm stacks) of cell-laden scaffolds were taken using a Nikon A1+ confocal microscope and merged. Six images/scaffold were captured at different locations and representative images are presented. To image large areas of the scaffold 50 z-stack images (2.5 μm stack) were taken using an UltraVIEW VoX Spinning Disc Confocal Microscope (PerkinElmer, Waltham, MA, USA) and the images were stitched together using the Volocity software (PerkinElmer). Myotube lengths were measured using the line tool measurement facility.

2.9. Scanning electron microscopy of scaffolds

The silk scaffolds (± HSMMs) were fixed in 4% PFA/PBS for 30 min at RT and then dehydrated in ethanol solutions of increasing concentration (30–100%) for 20 min per concentration, freeze dried using a ScanVac (LaboGene, Lynge, Denmark), mounted on aluminium stubs and sputter coated with platinum (5 nm) using a 208HR sputter coater (Cressington, Redding, CA, USA). The data were collected using either a Neon 40EsB scanning electron microscope (SEM) (Carl Zeiss, Oberkochen, Germany) or MIRA SEM (TESCAN, Brno, Czech Republic).

2.10. Rheological measurements of 3D silk scaffolds

Sample measurements were conducted using a HAAKE MARS III Modular Advanced Rheometer (Thermo Fisher Scientific, Waltham, MA, USA) with 35 mm diameter parallel plate geometry. Silk scaffolds (14 mm in diameter and 4 mm high) were fixed as described then hydrated in PBS. The gap height for the parallel plate arrangement was determined by monitoring the normal force, which was maintained at 0.3 ± 0.1 N during all measurements. The linear viscoelastic region, determined by performing stress sweep measurements, is the area where the moduli

DOI: 10.1002/term

values were independent of the applied stress or strain. The moduli values: elastic modulus (G′) and the viscous modulus (G′′), were determined in the linear viscoelastic region by strain sweep measurements. The stress sweep was performed from 1 to 70 Pa, the strain sweep was performed from 0.01–3% strain. Both sweeps were done at a frequency of 1 Hz and a temperature of 37°C. The data was analysed using HAAKE RheoWin software (version 3.61). The stress and strain values measured during the strain sweep (which correspond to the linear viscoelastic region for the scaffolds) were used to calculate Young's modulus. The stress was plotted against the strain and a linear regression was applied to the data. The gradient of the regression curve is equal to Young's modulus; the average value of four replicates was plotted as mean ± SD.

2.11. Alamar Blue assay for HSMM proliferation

HSMMs were cultured in the wells of a 48-well plate (Corning Inc., Corning, NY, USA) at a seeding density of 1×10^3cells/well in SkGM-2 medium/10% FBS (500 μl). After 2, 5, 8 and 11 days of proliferation on 2D substrates of a silk fibroin (10 μg/cm^2), or collagen I or fibronectin (10 μg/cm^2); or tissue culture plastic, 50 μl of Alamar Blue reagent (Life Technologies, Carlsbad, CA, USA) was added. The plates were incubated in a CO_2 incubator for 4 h and the fluorescence intensity measured using excitation and emission wavelengths of 560 nm and 590 nm, respectively, on an EnSpire Multimode plate reader (Perkin Elmer). Blank medium was the negative control and fluorescence units (RFU) relative to the control were calculated. Previous experiments indicated that the RFUs were in the linear range of an Alamar Blue standard curve obtained by titrating cell numbers.

2.12. Etching of glass coverslips

Glass coverslips (13 mm diameter; ProScitech, Thuringowa, Australia) that had been stored in 100% ethanol were treated with etch solution [6.0 g NaOH dissolved in 24 ml double distilled (dd) H_2O and the volume made up to 60 ml with 95% ethanol] for 30 min at RT. Coverslips were then washed with ddH_2O, dried at RT and sterilized by UV light.

2.13. Immunofluorescent staining of myoblasts in 2D culture

The HSMMs in SkGM-2 medium were seeded (15×10^3/cm^2) on etched glass coverslips coated with fibroin, collagen type I or fibronectin (coating concentration 10 μg/cm^2) and cultured for 3 days. The medium was changed to differentiation medium (DMEM/F12/2% HS). After day 7 or 10 of differentiation cells were fixed in 4% PFA/PBS, permeabilized with 0.1% Triton X-100/PBS at RT and blocked using 10% FBS/1% BSA/PBS (blocking solution) for 1 h. Cells were incubated with the anti-MyHCB mAb and the GLUT4 antibody diluted in blocking solution for 2 h at RT, washed with PBS and incubated for 1 h in AF488-conjugated goat anti-mouse antibody and AF546-conjugated goat anti-rabbit antibody diluted in blocking solution. The coverslips were washed and mounted in 4′,6-diamidino-2-phenylindole (DAPI)-containing Vectashield. Fluorescent images were captured using a Axioskop microscope (Carl Zeiss) with a × 40 objective and Spot Advanced software (SPOT imaging solutions, Sterling Heights, MI, USA). Nuclei and myotubes were counted in six random fields of view (>250 nuclei) and fusion index (FI) was calculated according to the formula: FI = (number of nuclei within myotubes containing ≥2 nuclei/total number of nuclei) × 100. Two independent experiments were performed and representative data are shown.

2.14. Quantitative real-time reverse transcription polymerase chain reaction (qRT-PCR) of muscle differentiation genes

Total mRNA was isolated using TRI Reagent (Sigma-Aldrich) as per the manufacturer's instructions from HSMMs cultured on *B. mori* and *A. mylitta* scaffolds (seeded at 5×10^5 cells/scaffold) in SkGM-2 media and differentiated in DMEM/F12/HS as described. mRNA concentration and purity was assessed using a Nanodrop spectrophotometer (Thermo Fisher Scientific). All mRNA samples had an A260/A280 ratio of >1.8. Reverse transcription was performed on 500 ng of mRNA using the Tetro cDNA synthesis kit (Bioline, Alexandria, Australia) as instructed by the manufacturer. A qRT-PCR was performed on cDNA prepared from differentiation day 0 (day 4 of proliferation, immediately before triggering differentiation) and differentiation day 4, with gene

Table 2. Primer Information

Gene	Sequence (5′–3′)	NCBI ref.	Primer Bank ID	T_M (°C)	Length (bp)
SDHA	F: TGG CAT TTC TAC GAC ACC GTGR: GCC TGC TCC GTC ATG TAG TG	NM_004168	156416002c3	54, 56	77
ACTAB	F: CATGTACGTTGCTATCCAGGC R: CTCCTTAATGTCACGCACGAT	NM_001101	4501885a1	61, 60	250
TBP	F: CCC GAA ACG CCG AAT R: ATA ATC CAAT CAG TGC CGT GGT TCG TG	NM_003194	285026518c2	55, 54	80
MYOD1	F: CGG CAT GAT GGA CTA CAG CGR: CAG GCA GTC TAG GCT CGA C	NM_002478	77695919c2	56, 55	133
MYF5	F: CTG CCA GTT CTC ACC TTC TGAR: AAC TCG TCC CCA AAT TCA CCC	NM_005593	156104905c1	54, 54	78
ACTA1	F: GGC ATT CAC GAG ACC ACC TACR: CGA CAT GAC GTT GTT GGC ATA C	NM_002478	47078293c1	56, 55	84
MYH1	F: GGG AGA CCT AAA ATT GGC TCA AR: TTG CAG ACC GCT CAT TTC AAA	NM_005963	115527081c2	53, 50	106
MYH7	F: TGG ATG TGA GTG AAC TTG GGGR: GCA CCC AGA CTC GCT TCT T	NM_020884	291045202c2	54, 53	108

F, forward; R, reverse.

DOI: 10.1002/term

expression levels normalized to the baseline expression at day 0, and from cDNA prepared on differentiation days 2 and 10, with gene expression on day 10 normalized to expression on day 2. The qRT-PCR reactions were performed using SensiFAST SYBR Lo-Rox kit (Bioline), with triplicate reactions containing 5 μl SYBR Green Lo-RoX Mix, 2 μl template cDNA, 1 μl forward/reverse primer (25 ng/μl) and 2 μl RNase free H_2O. The reactions were performed on a ViiA™ 7 Real-Time PCR system (Applied Biosystems, Life Technologies) with fast 96-well block using the cycling conditions: denaturation at 95°C for 2 min, 40 cycles of denaturation at 95°C for 5 s and annealing and extension together in one step at 60°C for 20 s followed by a melt step ranging from 55 to 95°C. Primers (Table 2) were selected for three reference genes [succinate dehydrogenase complex, subunit A (*SDHA*), beta actin (*ACTAB*), TATA-binding protein (*TBP*)] and five genes of interest for muscle transcription factors [myogenic factor 5 (*Myf5*), myogenic determinant protein-1 (*MyoD1*), heavy chain myosin (*MYH1* and *MYH7*) and skeletal muscle alpha actin (*ACTA1*)] using the PrimerBank database (Spandidos *et al*., 2010) and purchased from Geneworks (Hindmarsh, Australia). Of the reference genes, *TBP* had the most stable expression according to Normfinder (Andersen *et al*., 2004) and Bestkeeper (Pfaffl *et al*., 2004) software and was used as the reference gene. TBP is a central regulatory eukaryotic transcription factor, used by cellular RNA polymerases and is a stable reference gene for HSMMs under differentiation conditions (Stern-Straeter *et al*., 2009). The expression levels for *MyoD1*, *Myf5*, *MYH1*, *MYH7* and *ACTA1* were normalized to *TBP* expression values and fold-change determined using the 2-delta delta Ct method with baseline expression at differentiation day 0 set at 1. The mean ± standard error of four replicates are provided.

2.15. Statistical analysis

The data from three to four independent replicates per data point were collected from duplicate experiments and represented as means ± standard deviations. Analysis of cell proliferation experiments and rheology measurements was performed using one-way analysis of variance (ANOVA) followed by Tukey's *post-hoc* test, after

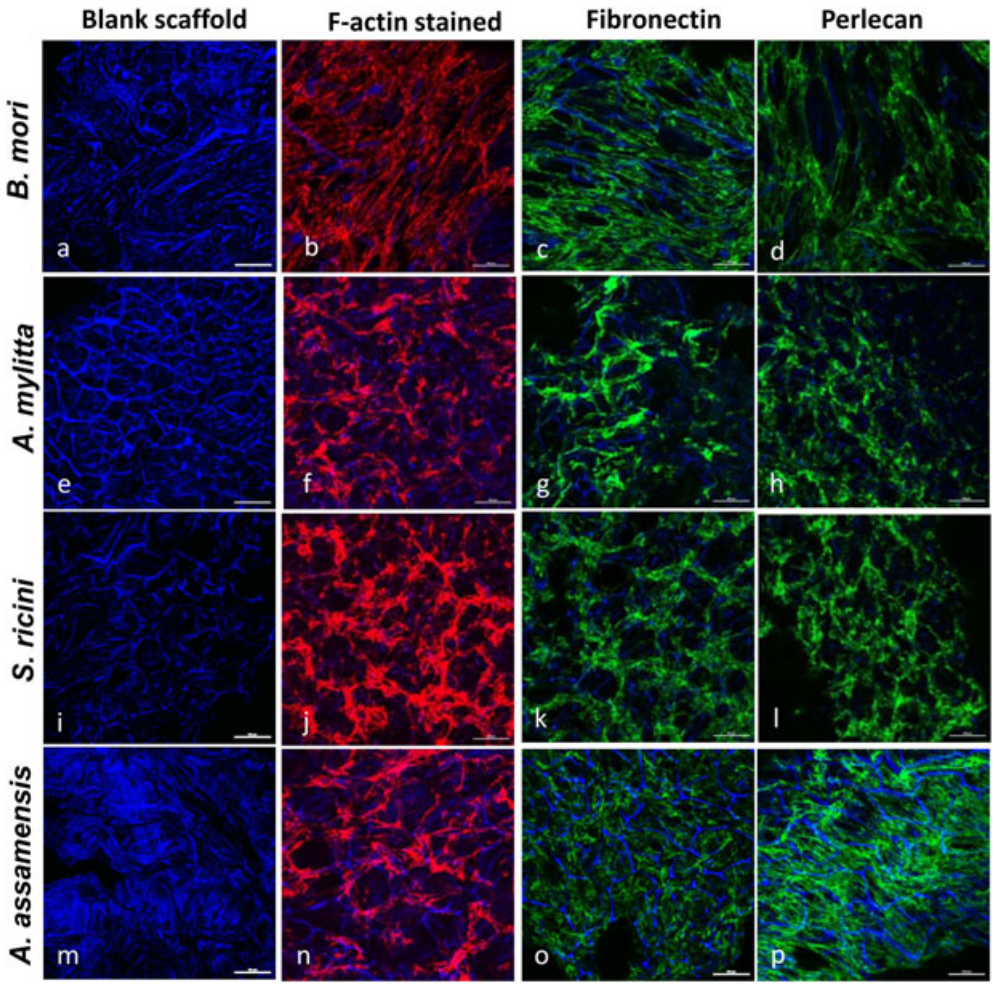

Figure 2. Human skeletal muscle myoblasts (HSMMs) adhere and secrete extracellular matrix (ECM) proteins on three-dimensional (3D) silk scaffolds. The HSMMs were cultured on 3D silk scaffolds for 2 days in skeletal muscle growth medium-2 proliferation medium, then fixed and stained with rhodamine–phalloidin (F-actin staining; b,f,j,n), or antibodies recognizing either fibronectin (c,g,k,o), or perlecan (d,h,l,p). 4′,6-diamidino-2-phenylindole (DAPI) stained the silk scaffolds (all panels). Images were captured using a Nikon A1 confocal laser scanning microscope. The merged images of several z-stack images (5 μm each stack, 150–200 μm deep into the scaffold) are presented. A representative image of six fields of view is shown. Bar: 50 μm

DOI: 10.1002/term

the data were confirmed to have a normal distribution using the Shapiro–Wilk test. Statistical analyses of qRT-PCR data were performed using the non-parametric Mann–Whitney *U*-test, because these data have a non-normal distribution.

3. Results

3.1. The interaction of HSMMs with the silk 3D scaffolds

At 2 days after seeding HSMMs in proliferation medium onto the scaffolds, rhodamine–phalloidin staining of polymerized actin fibres revealed that these cells had adhered to all four scaffold types and were covering the scaffold surfaces (Figure 2). The F-actin fibre arrangement indicated the cells were well spread on all scaffolds. On *A. mylitta*, *S. ricini* or *A. assamensis* scaffolds the cells appeared to be oriented around the scaffold pores (Figure 2f,j,n), whereas on *B. mori* scaffolds a different F-actin arrangement was apparent, with actin fibres oriented in parallel and, in places, crossing over the pores (Figure 2b). Staining of unseeded scaffolds revealed their porosity (Figure 2a,e,i,m). Immunostaining of HSMMs on 3D scaffolds revealed deposition of both fibronectin and perlecan. The staining intensities suggested comparable deposition of these molecules on all four scaffolds (Figure 2). The organization of the matrix proteins largely mirrored the F-actin fibre arrangement, although this is less apparent on *A. assamensis* scaffolds. A comparison of the fibronectin staining on the different scaffolds revealed fibronectin was deposited as parallel fibres on *B. mori* scaffolds (Figure 2c), whereas on *A. mylitta* and *S. ricini* scaffolds the fibronectin fibres were arranged in a circular pattern around the pores (Figure 2g,k).

3.2. HSMMs differentiation on 3D silk scaffolds

When stimulated with differentiation medium the HSMMs fused to form myotubes. Immunostaining with a mAb recognizing slow muscle myosin (MyHCB) revealed that multinucleated myotubes formed on all scaffolds (Figure 3), although there were markedly fewer myotubes on *S. ricini* scaffolds. Confocal imaging indicated that the myotubes were not necessarily confined to the same focal plane, suggesting they were formed by the fusion of cells at different depths in the scaffolds. The parallel alignment of the MyHCB-positive myotubes on *B. mori*, *A. mylitta* and *A. assamensis* scaffolds was striking. On *A. assamensis* scaffolds there appeared to be two layers of myotubes, one at a 90° orientation to the other. Confocal microscopy revealed that the area covered by the myotubes on *B. mori*

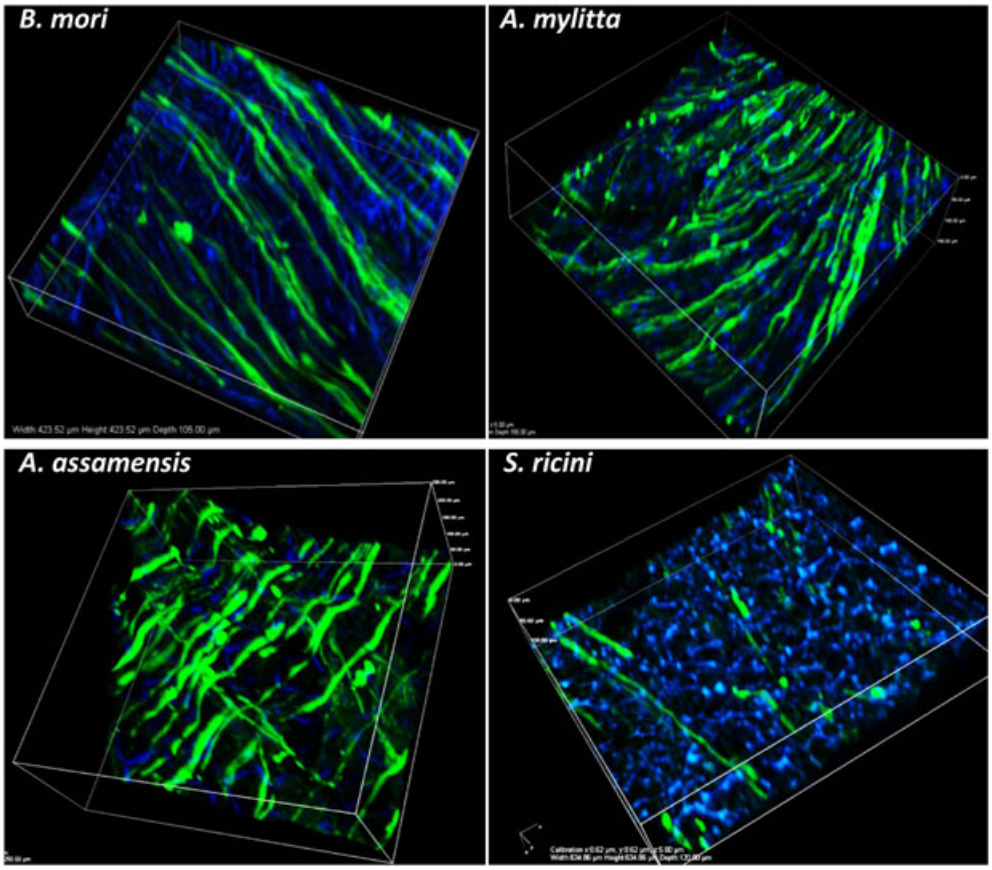

Figure 3. Immunostained images of differentiated human skeletal muscle myoblasts (HSMMs) on three-dimensional (3D) silk scaffolds. The HSMMs were cultured on the silk scaffolds for 4 days in proliferation medium and a further 4 days in differentiation medium. After differentiation, the scaffolds were stained with anti-myosin monoclonal antibody (NOQ7.5.4D) and goat anti-mouse IgG-AF488. The nuclei are stained with 4′,6-diamidino-2-phenylindole (DAPI, blue). Images were captured using a Nikon A1 confocal microscope. The 3D merged images of several z-stack images (5 μm each stack, 150–200 μm deep into scaffold) are represented. Bar: 100 μm

DOI: 10.1002/term

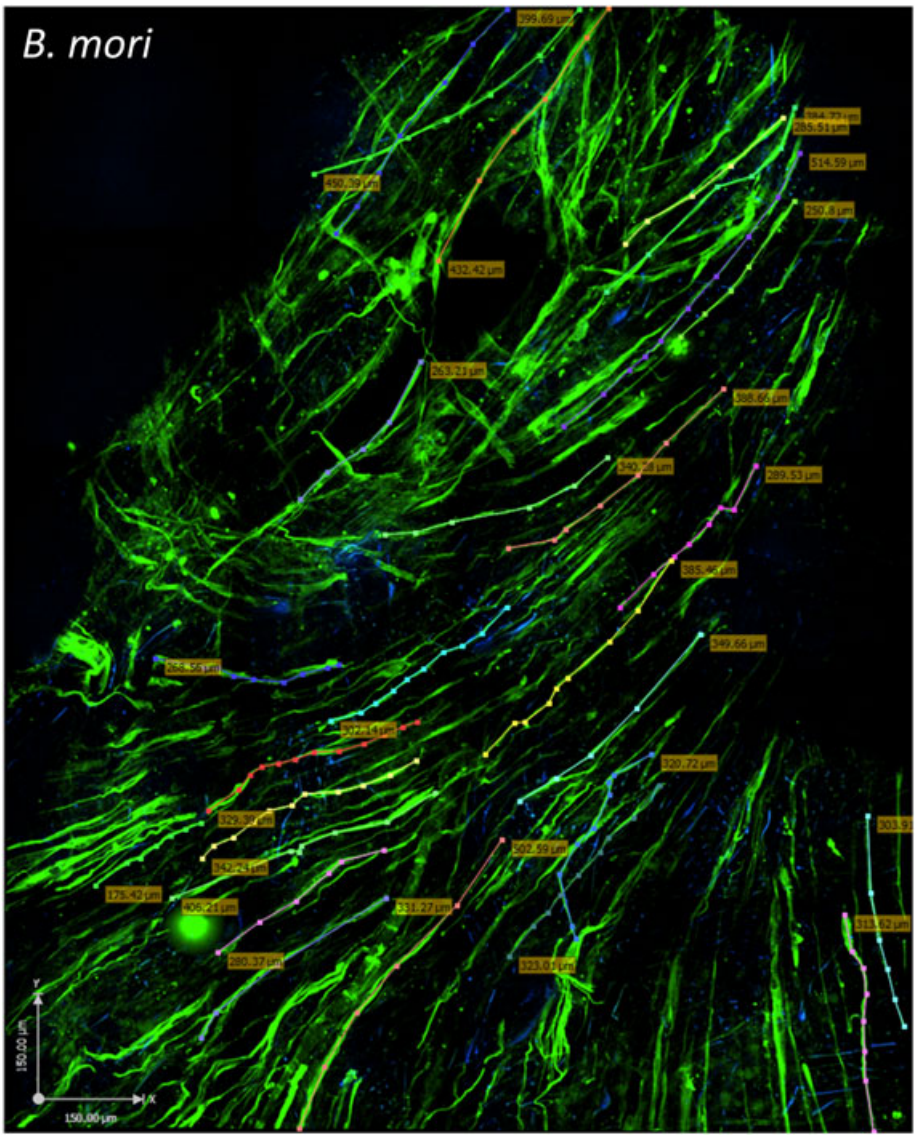

Figure 4. Human skeletal muscle myoblasts (HSMMs) form a three-dimensional (3D) muscle-like tissue on *Bombyx mori* scaffolds. The HSMMs were cultured for 4 days in skeletal muscle growth medium-2 proliferation medium and 4 days in differentiation medium on *B. mori* silk scaffolds. Myotubes were stained with anti-myosin monoclonal antibody (NOQ.5.4.D), followed by a goat anti-mouse AF488 conjugated second antibody. The images were captured using an Ultraview spinning disc confocal microscope (PerkinElmer). To capture a large area and estimate the coverage of the myotubes on the scaffold surface, 50 z-stack images (2.5 µm each stack) were stitched together using Volocity software. Muscle fibre length (coloured dotted lines and boxed numbers) was measured by tracing individual fibres using Volocity software. The area covered in this image is indicated by the following: *x*-axis, 1.58 mm; *y*-axis, 1.213 mm; z-stack, 125 µm. Bar: 150 µm

scaffolds was greater than that seen with the other scaffolds at identical cell seeding densities. In addition, as the longest myotubes formed on *B. mori* scaffolds, the length of these myotubes and the range in their lengths were determined. Measurements of 25 myotubes indicated an average length of 347 ± 7.2 µm and a range of 175–515 µm (Figure 4).

3.3. Ultrastructure and elastic properties of the 3D scaffolds

To determine if the ultrastructure of the scaffolds could have contributed to the differences in myotube formation, SEM was performed. All scaffolds had interconnecting pores, with diameters ranging from 50–120 µm on *A. mylitta*, 30–110 µm on *B. mori* and 30–90 µm on *S. ricini* and *A. assamensis* scaffolds, although *S. ricini* had a larger number of smaller pores than *A. assamensis* (Figure 5A;a, c,e,g). Despite these minor differences in pore size the HSMMs formed a continuous layer on all scaffolds, virtually covering the scaffold after 5 days (Figure 5A;b,d,f,h). On *A. assamensis* scaffolds, this appeared to consist of multiple cell layers (Figure 5A;h). Scanning electron microscopy of HSMMs on an *A. mylitta* scaffold revealed the cells were well spread, flat and elongated, with many contact points with the scaffold visible at 2 days after seeding (Figure 5B;b). The deposition of fibrous material, probably ECM proteins, onto the scaffold surface was also evident (Figure 5B;c).

Rheology measurements revealed the elastic properties of the silk scaffolds were quite different (Figure 6). The *B. mori* silk scaffolds had the highest Young's modulus with a mean value of 16.53 kPa followed by *A. mylitta* scaffolds with a mean value of 10.67 kPa, both of which were higher than those of *S. ricini* and

DOI: 10.1002/term

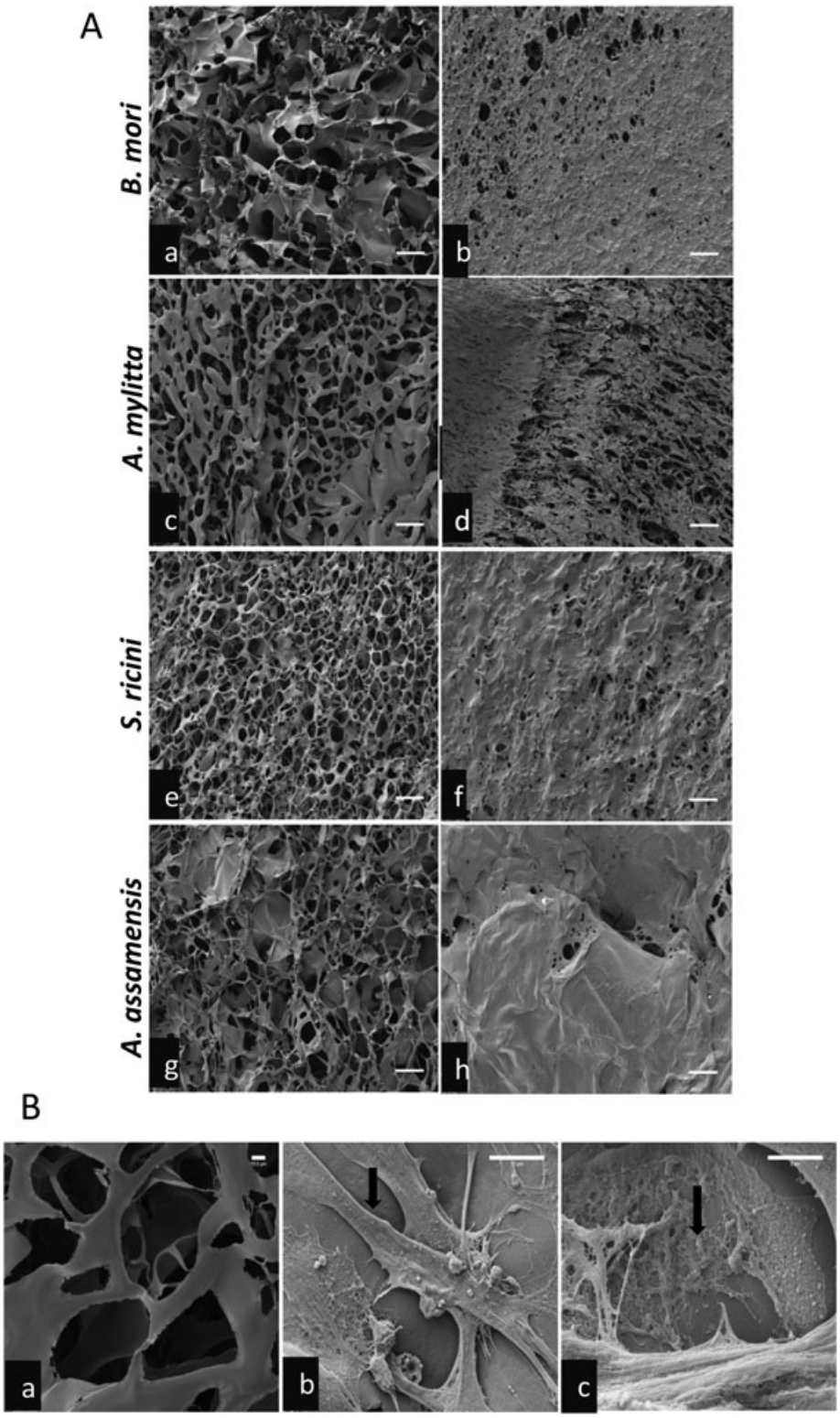

Figure 5. Scanning electron micrographs of three-dimensional (3D) silk scaffolds with and without human skeletal muscle myoblasts (HSMMs). (A) The scaffolds without cells (a, c, e, g) and at day 5 after seeding with HSMMs (b,d,f,h) are shown. Bars: 100 μm. (B) Highly magnified scanning electron micrographs of *Antheraea mylitta* silk scaffolds. The blank scaffold (a) shows the interconnected pores. HSMMs are shown at day 2 after seeding with a spread cell (b) indicated by arrow, and (c) matrix proteins deposited onto the scaffold (arrow). Bar: 10 μm (a,b), 2 μm (c)

A. assamensis scaffolds, which had similar Young's moduli (3.74 kPa and 3.73 kPa, respectively). A similar pattern was observed in the viscous modulus of the scaffolds with *B. mori* scaffolds having the highest viscous modulus and *S. ricini* scaffolds the lowest modulus (Figure 6).

3.4. Growth and differentiation of HSMMs on 2D silk fibroin substrates

To clarify whether amino acid composition differences in the fibroins could have affected the behaviour of the HSMMs, the proliferation and differentiation of these

DOI: 10.1002/term

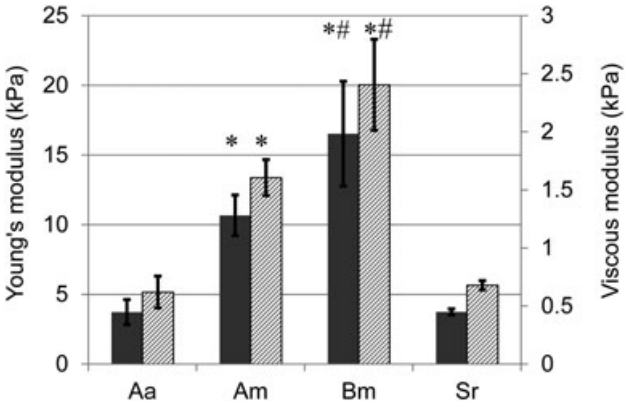

Figure 6. Young's modulus and viscous modulus of three-dimensional silk scaffolds. Strain sweep was performed from 0.01–3% at 1 Hz and 37°C. Scaffold dimensions were 14 mm in diameter and 4 mm thick and four replicate scaffolds were measured. Grey bars are Young's modulus (YM), hatched bars are viscous modulus (VM). Data are mean ± standard deviation (n = 4). Am, *Antheraea mylitta*; Bm, *Bombyx mori*; Aa, *Antheraea assamensis*; Sr, *Samia ricini*. *YM and VM are significantly greater in Am and Bm compared with Aa and Sr ($p \leq 0.01$); #YM and VM are significantly greater in Bm than Am ($p \leq 0.01$)

cells on 2D fibroin substrates was examined and compared with substrates of fibronectin and type I collagen. The 2D format was chosen to eliminate any confounding effects from scaffold structure differences. The growth and viability of HSMMs cultured for 11 days in SkGM-2 proliferation medium on the 2D substrates were measured using the Alamar Blue assay, which detects metabolic activity. The time-points chosen were days 2, 5, 8 and 11 as the doubling time of HSMMs was more than 42 h (data not shown). The HSMMs cultured on the silk fibroin and matrix protein substrates exhibited similar growth when subconfluent, at up to 8 days of culture (Figure 7). However, when the cells reached confluence (day 11), the assay measurements for HSMMs cultured on *A. mylitta* fibroin were significantly higher than those obtained from similarly cultured cells on the other substrates.

Immunostaining with an anti-MyHCB mAb of cells differentiated on 2D silk fibroin substrates revealed multinucleated myotubes with elongated nuclei (Figure 8).

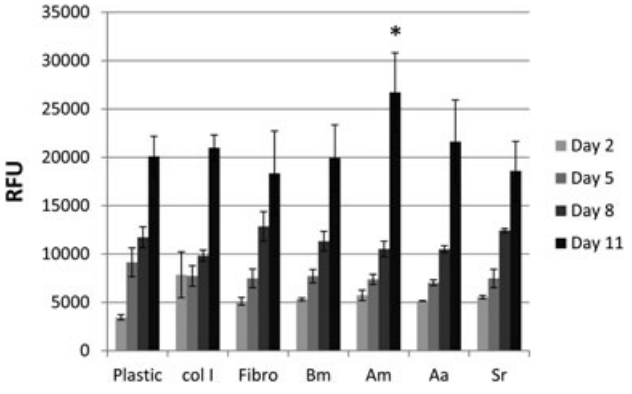

Figure 7. Human skeletal muscle myoblasts (HSMMs) are viable on silk fibroin substrates. Metabolic activity of HSMMs on four different silk fibroins, two extracellular matrix proteins and tissue culture plastic in Skeletal Muscle Growth Medium-2 was assessed using the Alamar Blue assay. The days in culture when the Alamar Blue dye was added and absorbance measured are indicated. The relative fluorescence units (RFU) were calculated relative to the control (media, no cells). Data are mean- standard deviation (n = 4). Am, *Antheraea mylitta*; Bm, *Bombyx mori*; Aa, *Antheraea assamensis*; Col I, collagen I; Fibro, Fibronectin; Sr, *Samia ricini*; *$p \leq 0.05$

These myotubes formed parallel to each other on all substrates by day 7 of differentiation and striations in the myotubes were visible by day 7 and remained at day 10. The staining pattern of an antibody to GLUT4, a glucose transporter protein and a marker of functional myotubes (Guillet-Deniau *et al*., 1994) revealed that GLUT4 was present along the length of the myotubes, although some perinuclear accumulation also occurred on all silk substrates (Figure 8e–h). To quantify differentiation, fusion indices of MyHCB-positive myotubes were determined (see the Supplementary material online, Figure A). The results show a similar percentage of nuclei within the myotubes, (77–81%) on collagen I, fibronectin and fibroins from *B. mori*, *A. mylitta* and *S. ricini*. However, on *A. assamensis* fibroin, the percentage of nuclei within the myotubes was significantly lower (57%) than that of HSMMs on the other substrates. The number of myotubes formed per field of view was also similar on collagen I, fibronectin and the fibroins from *B. mori*, *A. mylitta* and *S. ricini,* but on *A. assamensis* fibroin, fewer myotubes formed (see the Supplementary material online, Figure B).

3.5. Gene expression of myogenic markers in HSMMs on *B. mori* and *A. mylitta* 3D scaffolds

As the HSMMs readily formed myotubes on *B. mori* and *A. mylitta* fibroins in both the 3D scaffold and 2D film formats, cells grown on 3D scaffolds of these silk fibroins were selected for gene expression studies. The mRNA levels for muscle transcription factors (*Myf5* and *MyoD1*), heavy chain myosins (*MYH1* and *MYH7*), skeletal muscle alpha actin (*ACTA1*) and the reference gene (*TBP*) were determined by qRT-PCR. Gene expression by HSMMs in differentiation medium was examined at two sets of time-points to capture gene expression changes both early and late in myotube formation. Early gene expression was assessed at differentiation days 0 and 4, with day 4 data presented relative to expression levels at day 0 (Figure 9). On day 4, *Myf5* mRNA levels decreased and *MyoD1* expression increased on both scaffolds as the cells proceeded towards fusion and myotube formation (Figure 9a,b). A time-dependent increase was observed in *ACTA1, MYH1* and *MYH7* levels, indicative of maturing myotubes. The expression of the *ACTA1* gene was much higher on *A. mylitta* scaffolds than on *B. mori* scaffolds. The expression of these genes was also examined at differentiation day 10 relative to differentiation day 2, thereby detecting late gene expression changes. In this latter data set *ACTA1* expression in HSMMs at day 10 on *A. mylitta* scaffolds was significantly lower than that at day 2, whereas for the other genes, expression remained stable at day 2 and day 10. In contrast, on *B. mori* scaffolds the expression of *ACTA1* and *MYH1* was higher at day 10 than at day 2 (Figure 9c,d) and *Myf5* and *MyoD1* expression levels had decreased from day 10 to that at day 2. Collectively, these data suggest that HSMMs began to differentiate earlier on *A. mylitta* scaffolds than on *B. mori*

DOI: 10.1002/term

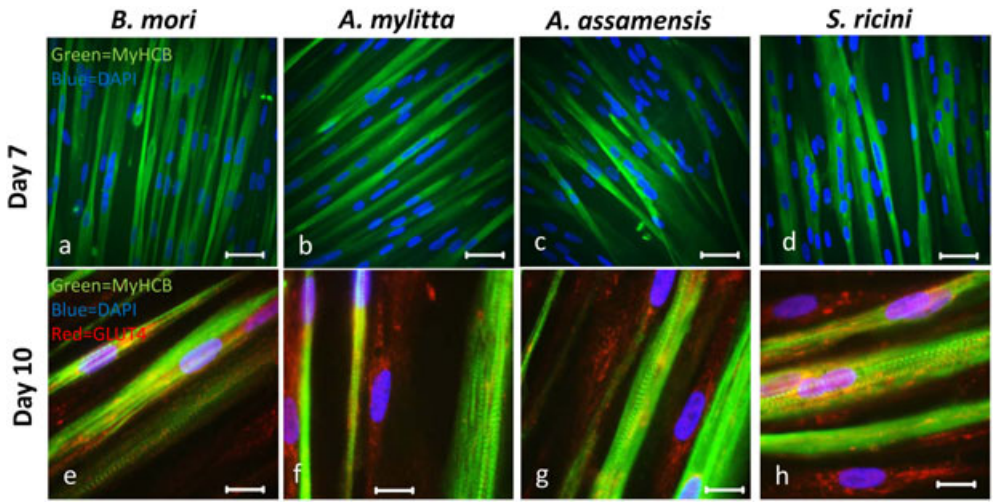

Figure 8. Human skeletal muscle myoblasts (HSMMs) differentiate to form myotubes on silk fibroin substrates. HSMMs were seeded on etched glass coated with the silk fibroins (10 μg/cm^2) and cultured for 4 days in skeletal muscle growth medium-2 proliferation medium and a further 7 or 10 days in differentiation medium. After 7 days of differentiation myotubes were stained with a mouse anti-myosin heavy chain monoclonal antibody (mAb) (NOQ7.5.4D) and goat anti-mouse IgG-AF488 (a–d) (MyHCB, mAb recognizing slow muscle myosin); after 10 days, myotubes were stained with both the anti-myosin mAb/goat anti-mouse IgG-AF488 combination and with rabbit anti-glucose transporter 4 (GLUT4) antibody followed by goat anti-rabbit IgG-AF546 (e–h). The nuclei were stained with 4′,6-diamidino-2-phenylindole (DAPI). Myotubes were imaged using a Zeiss Axioskop fluorescent microscope. Bar: 50 μm (a–d), 25 μm (e–h)

scaffolds, but the mature myotube gene expression pattern was lost at day 10, whereas on *B. mori* scaffolds it was maintained.

4. Discussion

The present study used four silk fibroins originating from different silkworm species to investigate what features are likely to be important in a 3D biomaterial for use in human skeletal muscle formation during regeneration. Those scaffolds that more closely resembled muscle in their elasticity (approximately 12–16 kPa) were best able to support myotube formation and alignment. Scaffolds of fibroin from *A. mylitta,* which has an RGD motif, did not enhance HSMM fusion and myotube formation over that seen with scaffolds of *B. mori* fibroin, which does not have an RGD sequence. Rather, the HSMMs adhered to, and deposited extensive ECMs on all of the 3D

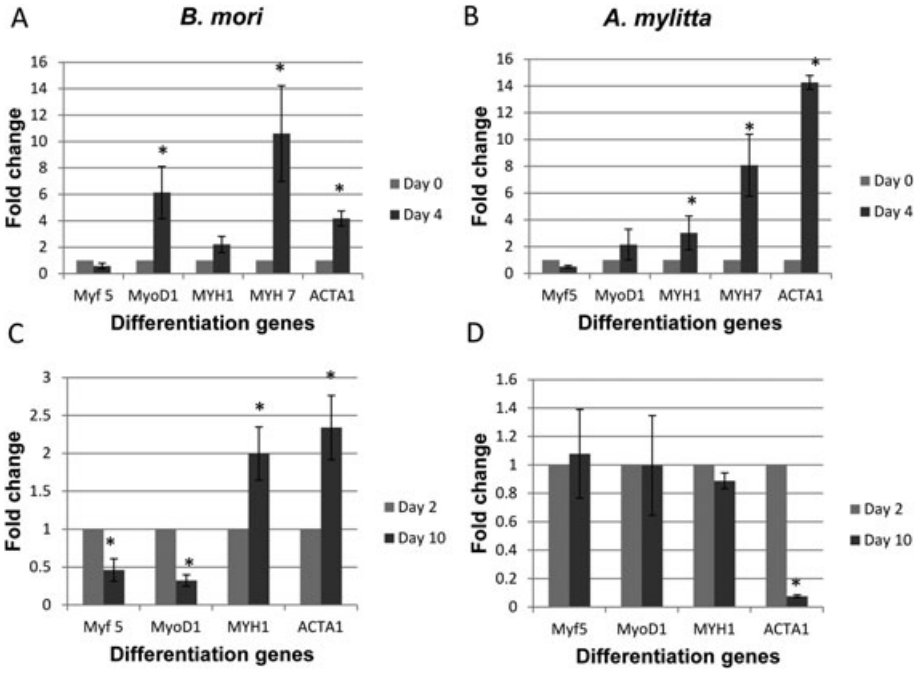

Figure 9. Quantitative real-time reverse transcription polymerase chain reaction (qRT-PCR) analysis reveals muscle differentiation on *Bombyx mori* and *Antheraea mylitta* three-dimensional (3D) silk scaffolds. qRT-PCR was used to determine the expression of five differentiation markers (Table 2) in HSMMs grown in skeletal muscle growth medium-2 on *Bombyx mori* (a,c) and *A mylitta* (b,d) scaffolds at day 4 (a,b) and day 10 (c,d) of differentiation. Relative expression levels for *MYF5*, *MYOD1*, *MYH1*, *MYH7* and *ACTA1* are normalized to the Ct value of the reference gene (*TBP*) and fold-change was determined using the using 2-delta delta Ct method. Day 4 and day 10 differentiation expression levels were normalized to day 0 and day 2 differentiation, respectively. The mean ± standard error of four biological replicates are presented. The Mann–Whitney *U*-test was performed and significance (p) values shown at each time-point for each gene using $^*p < 0.05$

DOI: 10.1002/term

scaffolds regardless of their fibroin composition. Nevertheless, the scaffolds did not equally support myotube formation and alignment, even though striated myotubes, expressing a functional marker, formed on 2D films of all fibroin types. When the length, alignment and gene expression pattern of the myotubes are considered, it is likely that scaffolds of *B. mori* fibroin will be the most useful for clinical applications involving skeletal muscle.

Other *in vitro* studies of silk as a biomaterial for skeletal muscle tissue engineering have only used fibroin from *B. mori* (Table 1) and most have used the immortalized murine myoblast cell line, C2C12 (Table 1). The present study used primary human myoblasts and four different silk fibroins and indicated that all the fibroins, when displayed in either a 2D or a 3D format, were compatible with HSMMs in tissue culture. On 3D silk scaffolds the HSMMs adhered to and spread on all scaffolds to form a cell sheet by day 5 in culture (Figures 2 and 5). Immunofluorescence analyses indicated that the HSMMs deposited ECM molecules on all of the silk scaffolds, a result supported by the SEM data of HSMMs on an *A. mylitta* scaffold (Figure 5B). These endogenous matrix proteins will interact with integrins on the cell surface of HSMMs to facilitate spreading and adhesion. Myoblasts express both the RGD binding integrins, α5β1, αvβ3 and αvβ5, as well as other non-RGD binding integrins including α3β1, α4β1, α4β7, α6β1 and α7β1 (García *et al*., 1999; Mayer, 2003). The rapid secretion of matrix proteins probably compensates for the absence of RGD peptides in some of the silk fibroins (Datta *et al*., 2001b), particularly as stable interactions mediated by α5β1 require another site in fibronectin, located adjacent to RGD (minimal sequence: PHSRN), and the αv integrins also bind to another site in fibronectin in addition to RGD (Leiss *et al*., 2008). As fibronectin assembles into fibrils at the cell surface bound to α5β1 or the αv integrins (Leiss *et al*., 2008), it is likely all of the silk fibroins provide a surface to which fibronectin fibrils can adsorb and this is what stabilizes cell adhesion and myotube formation on the different silk scaffolds. Others have similarly concluded that what is required for cell-self organization is a surface that facilitates cells to deposit and assemble their own, endogenous, adhesive ECM (Cerchiari *et al*., 2015).

These secreted ECM proteins are likely to have a role in myotube formation. A number of studies have reported a role for integrins in C2C12 cell myotube formation (García *et al*., 1999) and in an earlier study it was shown C2C12 cells very rapidly secreted fibronectin and perlecan under conditions of serum-free culture and formed myotubes (Chaturvedi *et al*., 2015). Data from *in vivo* animal models of muscle injury and repair indicate that fibronectin levels increase in regenerating areas of damaged muscle and there is increased production of collagen IV and the laminin α2 chain as the muscle myotubes mature (Grounds, 2008). Recent reviews also highlight the importance of fibronectin and perlecan (with its glycosaminoglycan chains), for muscle satellite cell self-renewal and skeletal muscle morphogenesis (Goody *et al*., 2015; Thomas *et al*., 2014). In a different system, silk/chitosan scaffolds modified by fibronectin and laminin deposited by Schwann cells initiated better repair of sciatic nerve injuries than non-coated scaffolds (Gu *et al*., 2014). Hence, biomaterials that trigger the resident cells to synthesize and deposit their own matrix may better support tissue repair.

Although there are differences in the capabilities of the fibroins to support myotube formation and alignment, this seemed to be because of the way the fibroins were presented to the cells rather than the composition of the fibroins *per se.* When the fibroins were used as a coating on tissue culture plastic, they all supported HSMM proliferation and differentiation, with only slight differences being evident. For example, the rapidly increased metabolic activity measured by the Alamar Blue assay in cells plated on *A. mylitta* fibroin suggested that these cells may have differentiated earlier than cells on the other three silk substrates (Figure 7), and the fusion indices and myotube numbers indicated that myotubes formed less well on *A. assamensis* films, but similarly on *B. mori, A. mylitta* and *S. ricini* fibroin films (Figure 8, and see the Supplementary material online, Figure S1). Interestingly, cell proliferation and myotube formation on the fibroin films was comparable to that seen on fibronectin and collagen I used at the same concentration and coating conditions (Figure 7 and Figure S1).

In contrast to the 2D format, the different fibroin 3D scaffolds supported HSMM myotube formation to varying degrees and this was quite apparent following immunostaining with an anti-MyHCB antibody (Figure 3). On *B. mori* scaffolds, HSMMs formed extremely long, well-aligned myotubes, whereas the myotubes that formed on *A. mylitta* scaffolds were thicker and shorter. The parallel alignment of HSMMs on *B. mori* scaffolds occurred by day 2 of proliferation, as revealed by the similar orientation of most of the F-actin fibres and by the orientation of the fibronectin fibrils (Figure 2). In contrast, on the other scaffolds the F-actin fibres tended to follow the edges of the scaffold pores, indicating that HSMMs on these scaffolds were not spanning the pores. Myotubes on *A. assamensis* fibroin scaffolds were predominately oriented in two perpendicular layers in an arrangement that will not favour a functioning skeletal muscle. The SEM images suggested multiple layers of cells on *A. assamensis* (Figure 5), whereas the cell layer was thinner on *A. mylitta* and *B. mori* scaffolds. Myosin expression was much lower in HSMMs seeded on the *S. ricini* fibroin scaffolds (Figure 3), suggesting that the architecture of these scaffolds was not ideal for myotube maturation.

The degree to which the HSMMs differentiated on the different scaffolds was examined by comparing the expression patterns of genes associated with myogenesis. *Myf5* is the first muscle-specific regulatory factor to be expressed during mouse embryogenesis while *MyoD1* promotes myoblasts cycle withdrawal and the induction of differentiation (Bentzinger *et al*., 2013). *MYH1* and *MYH7* are adult heavy chain myosin isoforms expressed in myotubes and myofibres, and *ACTA1* is a muscle actin isoform (Stern-Straeter *et al*., 2011). In the present study,

DOI: 10.1002/term

TBP was the most stable reference gene of those tested, which is in agreement with the study by Stern-Straeter *et al.* (2009).

The qRT-PCR data were consistent with the immunostaining data and indicated that HSMMs differentiated well on *A. mylitta* and *B. mori* scaffolds. On both scaffolds, a decrease in *Myf5* mRNA levels and an increase in *MyoD1* levels indicated that most myoblasts had begun to differentiate after 4 days in differentiation medium. The levels of *MYH7* mRNA were 8- to 10-fold higher at day 4, compared with day 0, which correlated with the strong myosin immunostaining of myotubes on both scaffolds (Figure 9). In contrast, *ACTA1* levels were much higher on *A. mylitta* than on *B. mori* at day 4 in differentiation medium, but by day 10 *ACTA1* mRNA levels in cells on *A. mylitta* scaffolds decreased relative to the levels at day 2, while the levels of expression of the other genes were similar to at both day 2 and day 10 (Figure 9). These data were quite different from those of cells on *B. mori* scaffolds and from the gene expression studies of human myoblast differentiation conducted by Stern-Straeter *et al.* (2011). The expression levels of all the genes examined at both the early and late differentiation stages on *B. mori* scaffolds were as expected from the earlier study (Stern-Straeter *et al*., 2011). Collectively these data suggest that although HSMMs started to differentiate more quickly on *A. mylitta* than on *B. mori* scaffolds, it appeared the myotubes that formed on *A. mylitta* scaffolds did not maintain their phenotype at the latter time-point. Possibly, the formation of long, well-aligned myotubes on *B. mori* scaffolds (Figure 8), occurred because on this scaffold, the gene expression pattern was characteristic of mature human muscle.

Pore size and the mechanical properties of scaffolds have been described as factors regulating cell proliferation and differentiation. Zhang *et al.* (2010) reported that human bone marrow mesenchymal stromal cells seeded on silk fibroin scaffolds showed greatest proliferation on scaffolds, with a pore size of 100–300 μm (Zhang *et al*., 2010). All the scaffolds used here have similar porosities, but the SEM indicated that the pore size of *S. ricini* (Figure 5A) was smaller than the other three scaffolds. Substrate stiffness or elasticity can also determine cell fate by altering mechanical signal transduction pathways (Engler *et al*., 2004, 2006). Possibly the HSMMs differentiated best on *B. mori* and *A. mylitta* scaffolds as these two scaffolds had a Young's modulus (E) of around 10–16 kPa, which is very close to the elastic modulus of human skeletal muscles (gastrocnemius and soleus) at rest (16.5 kPa and 14.5 kPa, respectively) (Shinohara *et al*., 2010) (Figure 6). There are no data on the Young's modulus of cultured HSMMs but for C2C12 myoblasts the Young's modulus is between 12 and 15 kPa (Collinsworth *et al*., 2002). The findings of the present study are consistent with those of Engler *et al.* (2004) who investigated the elastic properties of C2C12 myoblasts cultured on different substrates of varying stiffness (Engler *et al*., 2004). They found that although the myoblasts fused into myotubes irrespective of substrate flexibility, actin/myosin striations appeared only in myotubes cultured on gels with a stiffness close to normal muscle (Young's modulus: E ~ 12 kPa), indicating that substrate stiffness is a critical factor regulating myotube maturation (Engler *et al*., 2004). Later, the same group demonstrated the significance of matrix elasticity on stem cell fate (Engler *et al*., 2006). When mesenchymal stem cells (MSCs) were cultured on collagen-coated gels of varying elasticity that mimicked brain, muscle and bone matrix in their stiffness, they differentiated into myogenic cells on medium stiffness gels (E ~ 12 kPa), osteocytes on high-stiffness gels, and displayed neuronal morphology when cultured on matrices mimicking brain elasticity (Engler *et al*., 2006). Here it was shown that the viscous moduli of the two scaffolds that best supported myotube formation were similar and quite different from that of scaffolds from *S. ricini* and *A. assamensis*. These last two scaffolds either did not support differentiation or the myotubes that formed were not aligned in a single direction.

For some adult human skeletal muscles, individual myofibres may extend up to lengths of 35 cm, in parallel with the longitudinal orientation of the ECM (Paul, 2001; Harris *et al*., 2005). To form a functional new muscle *in vivo*, the implanted regenerated myofibres on the bioscaffold should fuse with the existing myofibres and become innervated. The *in vitro* data of the present study demonstrate that 3D fibroin scaffolds from *B. mori* supported HSMM differentiation into long, well-aligned myotubes, and are encouraging in this context. In contrast, short, thick myotubes formed on *A. mylitta* scaffolds suggesting that rapid differentiation may not produce the best myotubes.

5. Conclusion

Silk fibroins from four different silkworm species, under 2D and 3D culture conditions, effectively supported HSMM proliferation, myotube formation and maturation, although their efficacy differed. All the scaffolds stimulated the HSMMs to deposit an endogenous ECM and so the presence of an RGD motif in *A. mylitta* fibroin did not confer an advantage. Of greater importance for myotube formation and maturation was a scaffold elasticity that resembled that of normal muscle. This comparative study suggested that silk fibroin from the domesticated mulberry species, *B. mori*, when processed into a scaffold with elasticity similar to skeletal muscle, could be a useful biomaterial for skeletal muscle bioengineering, although fibroin from *A. mylitta* similarly prepared may also be useful. *Bombyx mori* silk fibroin materials are widely used and well tolerated in clinical situations, and this demonstration of the suitability of *B. mori* fibroin bioscaffolds, is a necessary first step for potential bioengineering of human skeletal muscle cells for future clinical applications.

DOI: 10.1002/term

Acknowledgments

The authors thank Prof. John Whitelock and Dr Megan Lord for the gift of the anti-perlecan antibody, CCN-1, and the assistance of Corey Giles in the preparation of Figure 7. This work was supported by a grant to DED and DRC from Defence Health Foundation, Australia and a Curtin University Early Career Research Fellowship to D.E.D. V.C. was supported by a Curtin University Strategic International Research Scholarship. The work was also supported by the Indian Council of Medical Research, Department of Biotechnology, and Government of India (S.C.K.). S.C. K. is grateful to Curtin University for providing all facilities during his visit to the School of Biomedical Science, Faculty of Health Sciences, Curtin University. The authors acknowledge the provision of research facilities and the scientific and technical assistance of the staff of both CHIRI Biosciences Research Precinct Core Facility and the Curtin University Electron Microscope Facility, which was partly funded by Curtin University, State and Commonwealth Governments. SC Kundu presently holds ERA Chair Full Professor of European Commission Programme (FoReCaST) at 3Bs Research Group, University of Minho, Portugal.

Conflict of interest

The authors have declared that there is no conflict of interest.

References

Andersen CL, Jensen JL, Ørntoft TF. 2004; Normalization of real-time quantitative reverse transcription-PCR data: a model-based variance estimation approach to identify genes suited for normalization, applied to bladder and colon cancer data sets. *Cancer Res* **64**: 5245–5250.

Banani K, Kundu SC. 2013; Bio-inspired fabrication of fibroin cryogels from the muga silkworm *Antheraea assamensis* for liver tissue engineering. *Biomed Mater* **8**: 055003. DOI: 10.1088/1748-6041/8/5/.

Bauer F, Wohlrab S, Scheibel T. 2013; Controllable cell adhesion, growth and orientation on layered silk protein films. *Biomater Sci* **1**: 1244–1249.

Bentzinger CF, Wang YX, Dumont NA, *et al*. 2013; Cellular dynamics in the muscle satellite cell niche. *EMBO Rep* **14**: 1062–1072.

Bhardwaj N, Nguyen QT, Chen AC, *et al*. 2011; Potential of 3-D tissue constructs engineered from bovine chondrocytes/silk fibroin-chitosan for *in vitro* cartilage tissue engineering. *Biomaterials* **32**: 5773–5781.

Bhardwaj N, Sow WT, Devi D, *et al*. 2015; Silk fibroin-keratin based 3D scaffolds as a dermal substitute for skin tissue engineering. *Integr Biol (Camb)* **7**: 53–63.

Cerchiari AE, Garbe JC, Jee NY, *et al*. 2015; A strategy for tissue self-organization that is robust to cellular heterogeneity and plasticity. *Proc Natl Acad Sci* **112**: 2287–2292.

Chaturvedi V, Dye DE, Kinnear BF, *et al*. 2015; Interactions between skeletal muscle myoblasts and their extracellular matrix revealed by a serum free culture system. *PLoS One* **10**: e0127675. DOI: 10.1371/journal.pone.

Collinsworth AM, Zhang S, Kraus WE, Truskey, GA. 2002; Apparent elastic modulus and hysteresis of skeletal muscle cells throughout differentiation. *Am J Physiol Cell Physiol* **283**: C1219–C1227.

Datta A, Ghosh AK, Kundu CS. 2001a; Purification and characterization of fibroin from the tropical Saturniid silkworm, *Antheraea mylitta*. *Insect Biochem Mol Biol* **31**: 1013–1018.

Datta A, Ghosh AK, Kundu, SC. 2001b; Differential expression of the fibroin gene in developmental stages of silkworm, *Antheraea mylitta* (Saturniidae). *Comp Biochem Physiol B Biochem Mol Biol* **129**: 197–204.

Engler AJ, Griffin MA, Sen S, *et al*. 2004; Myotubes differentiate optimally on substrates with tissue-like stiffness: pathological implications for soft or stiff microenvironments. *J Cell Biol* **166**: 877–887.

Engler AJ, Sen S, Sweeney HL, *et al*. 2006; Matrix elasticity directs stem cell lineage specification. *Cell* **126**: 677–689.

Fu C, Shao Z, Fritz V. 2009; Animal silks: their structures, properties and artificial production. *Chem Commun* **43**: 6515–6529.

Fujita H, Endo A, Shimizu K, Nagamori, E. 2010; Evaluation of serum-free differentiation conditions for C2C12 myoblast cells assessed as to active tension generation capability. *Biotechnol Bioeng* **107**: 894–901.

García AJ, Vega MD, Boettiger D. 1999; Modulation of cell proliferation and differentiation through substrate-dependent changes in fibronectin conformation. *Mol Biol Cell* **10**: 785–798.

Gentile NE, Stearns KM, Brown EH, *et al*. 2014; Targeted rehabilitation after extracellular matrix scaffold transplantation for the treatment of volumetric muscle loss. *Am J Phys Med Rehabil* **93**: S79–S87.

Goody MF, Sher RB, Henry CA. 2015; Hanging on for the ride: adhesion to the extracellular matrix mediates cellular responses in skeletal muscle morphogenesis and disease. *Dev Biol* **401**: 75–91.

Grogan BF. Hsu JR, Skeletal Trauma Research, C. 2011; Volumetric muscle loss. *J Am Acad Orthop Surg* **19**(Suppl 1): S35–S37.

Grounds, MD. 2008; Complexity of extracellular matrix and skeletal muscle regeneration. In Skeletal Muscle Repair and Regeneration (SS Schiaffino, TT Partridge eds). Springer Amsterdam.

Grounds MD. 2014; Therapies for sarcopenia and regeneration of old skeletal muscles. *BioArchitecture* **4**: 81–87.

Gu Y, Zhu J, Xue C, *et al*. 2014; Chitosan/silk fibroin-based, Schwann cell-derived extracellular matrix-modified scaffolds for bridging rat sciatic nerve gaps. *Biomaterials* **35**: 2253–2263.

Guillet-Deniau I, Leturque A, Girard J. 1994; Expression and cellular localization of glucose transporters (GLUT1, GLUT3, GLUT4) during differentiation of myogenic cells isolated from rat foetuses. *J Cell Sci* **107**: 487–496.

Harris AJ, Duxson MJ, Butler JE, *et al*. 2005; Muscle fiber and motor unit behavior in the longest human skeletal muscle. *J Neurosci* **25**: 8528–8533.

Horan RL, Antle K, Collette AL, *et al*. 2005; *In vitro* degradation of silk fibroin. *Biomaterials* **26**: 3385–3393.

Hu X, Park S-H, Gil ES, *et al*. 2011; The influence of elasticity and surface roughness on myogenic and osteogenic-differentiation of cells on silk-elastin biomaterials. *Biomaterials* **32**: 8979–8989.

Kar S, Talukdar S, Pal S, *et al*. 2013; Silk gland fibroin from indian muga silkworm Antheraea assama as potential biomaterial. *Tissue Eng Regen Med* **10**: 200–210.

Kim HJ, Kim U-J, Kim HS, *et al*. 2008; Bone tissue engineering with premineralized silk scaffolds. *Bone* **42**: 1226–1234.

Kundu B, Rajkhowa R, Kundu SC, Wang, X. 2013; Silk fibroin biomaterials for tissue regenerations. *Adv Drug Deliv Rev* **65**: 457–470.

Kundu SC, Kundu B, Talukdar S, *et al*. 2012a; Invited review nonmulberry silk biopolymers. *Biopolymers* **97**: 455–467.

Kundu SC, Kundu B, Talukdar S, *et al*. 2012b; Nonmulberry silk biopolymers. *Biopolymers* **97**: 455–467.

Leiss M, Beckmann K, Girós A, *et al*. 2008; The role of integrin binding sites in fibronectin matrix assembly *in vivo*. *Curr Opin Cell Biol* **20**: 502–507.

Li M, Ogiso M, Minoura, N. 2003; Enzymatic degradation behavior of porous silk fibroin sheets. *Biomaterials* **24**: 357–365.

Mahendran B, Ghosh SK, Kundu, SC. 2006; Molecular phylogeny of silk-producing insects based on 16S ribosomal RNA and cytochrome oxidase subunit I genes. *J Genet* **85**: 31–38.

Mase VJ Jr, Hsu JR, Wolf SE, *et al*. 2010; Clinical application of an acellular biologic scaffold for surgical repair of a large, traumatic quadriceps femoris muscle defect. *Orthopedics* **33**: 511.

Mayer, U. 2003; Integrins: redundant or important players in skeletal muscle? *J Biol Chem* **278**: 14587–14590.

Meinel L, Kaplan, DL. 2012; Silk constructs for delivery of musculoskeletal therapeutics. *Adv Drug Deliv Rev* **64**: 1111–1122.

Meinel L, Fajardo R, Hofmann S, Langer R, Chen J, Snyder B, Vunjak-Novakovic G, Kaplan, D. 2005; Silk implants for the healing of critical size bone defects. *Bone* **37**: 688–698.

Morgan AW, Roskov KE, Lin-Gibson S, *et al*. 2008; Characterization and optimization of RGD-containing silk blends to support osteoblastic differentiation. *Biomaterials* **29**: 2556–2563.

Nazarov R, Jin, H.-J, Kaplan, DL. 2004; Porous 3-D scaffolds from regenerated silk fibroin. *Biomacromolecules* **5**: 718–726.

Omenetto FG, Kaplan, DL. 2010; New opportunities for an ancient material. *Science* **329**: 528–531.

Pal S, Kundu J, Talukdar S, *et al*. 2013; An emerging functional natural silk biomaterial from the only domesticated non-mulberry silkworm *Samia ricini*. *Macromol Biosci* **13**: 1020–1035.

Park H-S, Gong M-S, Park J-H, *et al*. 2013a; Silk fibroin–polyurethane blends: physical properties and effect of silk fibroin content on viscoelasticity, biocompatibility and myoblast differentiation. *Acta Biomater* **9**: 8962–8971.

Park H-S, Gong M-S, Park J-H, *et al*. 2013b; Silk fibroin–polyurethane blends: physical properties and effect of silk fibroin content on viscoelasticity, biocompatibility and myoblast differentiation. *Acta Biomater* **9**: 8962–8971.

Patra C, Talukdar S, Novoyatleva T, *et al*. 2012; Silk protein fibroin from *Antheraea mylitta* for cardiac tissue engineering. *Biomaterials* **33**: 2673–2680.

Paul AC. 2001; Muscle length affects the architecture and pattern of innervation differently in leg muscles of mouse, guinea pig, and rabbit compared to those of human and monkey muscles. *Anat Rec* **262**: 301–309.

Pfaffl M, Tichopad A, Prgomet C, *et al*. 2004; Determination of stable housekeeping genes, differentially regulated target genes and sample integrity: BestKeeper – Excel-based tool using pair-wise correlations. *Biotechnol Lett* **26**: 509–515.

Shen Z, Guo S, Ye D, *et al*. 2013; Skeletal muscle regeneration on protein-grafted and microchannel-patterned scaffold for hypopharyngeal tissue engineering. *Biomed Res Int* **2013**: 8.

Shinohara M, Sabra K, Gennisson J-L, *et al*. 2010; Real-time visualization of muscle stiffness distribution with ultrasound shear wave imaging during muscle contraction. *Muscle Nerve* **42**: 438–441.

Sicari BM, Rubin JP, Dearth CL, *et al*. 2014; An acellular biologic scaffold promotes skeletal muscle formation in mice and humans with volumetric muscle loss. *Sci Transl Med* **6**: 234ra58.

Sofia S, McCarthy MB, Gronowicz G, *et al*. 2001; Functionalized silk-based biomaterials for bone formation. *J Biomed Mater Res* **54**: 139–148.

Spandidos A, Wang X, Wang H, *et al*. 2010; PrimerBank: a resource of human and mouse PCR primer pairs for gene expression detection and quantification. *Nucleic Acids Res* **38**: D792–D799.

Stern-Straeter J, Bonaterra G, Hormann K, *et al*. 2009; Identification of valid reference genes during the differentiation of human myoblasts. *BMC Mol Biol* **10**: 66.

Stern-Straeter J, Bonaterra GA, Kassner SS, *et al*. 2011; Characterization of human myoblast differentiation for tissue-engineering purposes by quantitative gene expression analysis. *J Tissue Eng Regen Med* **5**: e197–e206.

Talukdar S, Nguyen QT, Chen AC, *et al*. 2011; Effect of initial cell seeding density on 3D-engineered silk fibroin scaffolds for articular cartilage tissue engineering. *Biomaterials* **32**: 8927–8937.

Tanaka K, Inoue S, Mizuno S. 1999; Hydrophobic interaction of P25, containing Asn-linked oligosaccharide chains, with the H–L complex of silk fibroin produced by *Bombyx mori*. *Insect Biochem Mol Biol* **29**: 269–276.

Tang-Schomer MD, White JD, Tien LW, *et al*. 2014; Bioengineered functional brain-like cortical tissue. *Proc Natl Acad Sci* **111**: 13811–13816.

Thomas K, Engler AJ, Meyer, GA. 2014; Extracellular matrix regulation in the muscle satellite cell niche. *Connect Tissue Res* **56**: 1–8.

Wang L, Cao L, Shansky J, *et al*. 2014; Minimally invasive approach to the repair of injured skeletal muscle with a shape-memory scaffold. *Mol Ther* **22**: 1441–1449.

Wang Y, Rudym DD, Walsh A, *et al*. 2008; *In vivo* degradation of three-dimensional silk fibroin scaffolds. *Biomaterials* **29**: 3415–3428.

Yucel T, Lovett ML, Kaplan DL. 2014; Silk-based biomaterials for sustained drug delivery. *J Control Release* **190**: 381–397.

Zhang Y, Fan W, Ma Z, *et al*. 2010; The effects of pore architecture in silk fibroin scaffolds on the growth and differentiation of mesenchymal stem cells expressing BMP7. *Acta Biomater* **6**: 3021–3028.

Zhou C-Z, Confalonieri F, Medina N, *et al*. 2000; Fine organization of *Bombyx mori* fibroin heavy chain gene. *Nucleic Acids Res* **28**: 2413–2419.

Zhou J, Cao C, Ma X, *et al*. 2010; *In vitro* and *in vivo* degradation behavior of aqueous-derived electrospun silk fibroin scaffolds. *Polymer Degrad Stabil* **95**: 1679–1685.

Supporting information

Additional supporting information may be found in the online version of this article at the publisher's web-site.

DOI: 10.1002/term